

Is MRI-Based CFD Able to Improve Clinical Treatment of Coarctations of Aorta?

L. GOUBERGRITS,^{1,2} E. RIESENKAMPFF,² P. YEVTUSHENKO,¹ J. SCHALLER,¹ U. KERTZSCHER,¹ F. BERGER,²
and T. KUEHNE^{2,3}

¹Biofluid Mechanics Laboratory, Charité – Universitätsmedizin Berlin, Augustenburger Platz 1, Berlin 13353, Germany; ²Department of Congenital Heart Disease and Pediatric Cardiology, Deutsches Herzzentrum Berlin, Augustenburger Platz 1, 13353 Berlin, Germany; and ³Non-Invasive Cardiac Imaging in Congenital Heart Disease Unit, Charité – Universitätsmedizin Berlin, Augustenburger Platz 1, Berlin 13353, Germany

(Received 6 May 2014; accepted 6 September 2014; published online 16 September 2014)

Associate Editor Diego Gallo oversaw the review of this article.

Abstract—Pressure drop associated with coarctation of the aorta (CoA) can be successfully treated surgically or by stent placement. However, a decreased life expectancy associated with altered aortic hemodynamics was found in long-term studies. Image-based computational fluid dynamics (CFD) is intended to support particular diagnoses, to help in choosing between treatment options, and to improve performance of treatment procedures. This study aimed to prove the ability of CFD to improve aortic hemodynamics in CoA patients. In 13 patients (6 males, 7 females; mean age 25 ± 14 years), we compared pre- and post-treatment peak systole hemodynamics [pressure drops and wall shear stress (WSS)] vs. virtual treatment as proposed by biomedical engineers. Anatomy and flow data for CFD were based on MRI and angiography. Segmentation, geometry reconstruction and virtual treatment geometry were performed using the software ZIBAmira, whereas peak systole flow conditions were simulated with the software ANSYS® Fluent®. Virtual treatment significantly reduced pressure drop compared to post-treatment values by a mean of 2.8 ± 3.15 mmHg, which significantly reduced mean WSS by 3.8 Pa. Thus, CFD has the potential to improve post-treatment hemodynamics associated with poor long-term prognosis of patients with coarctation of the aorta. MRI-based CFD has a huge potential to allow the slight reduction of post-treatment pressure drop, which causes significant improvement (reduction) of the WSS at the stenosis segment.

Keywords—Aortic coarctation, Computational fluid dynamics, Magnetic resonance imaging, Virtual treatment, Wall shear stress, Pressure drop.

ABBREVIATIONS

CoA	Coarctation of the aorta
TCC	Total cavopulmonary connections
MRI	Magnetic resonance imaging
VEC-MRI	Velocity-encoded MRI
WH	Whole heart
CFD	Computational fluid dynamics
WSS	Wall shear stress
3D	Three-dimensional
4D	Four-dimensional
SD	Standard deviation
DS	Degree of stenosis

INTRODUCTION

Coarctation of the aorta (CoA) associated with increased blood pressure in the upper body and decreased pressure in the lower body represents about 10% of congenital heart diseases.¹³ In spite of successful treatment (surgical or catheter-based) of the pressure drop caused by a coarctation, a long-term prognosis is associated with decreased life expectancy. This is supposed to be explained by abnormal hemodynamics of the aorta.²³ Image-based computational fluid dynamics (CFD) analysis of hemodynamics in

Address correspondence to L. Goubergrits, Department of Congenital Heart Disease and Pediatric Cardiology, Deutsches Herzzentrum Berlin, Augustenburger Platz 1, 13353 Berlin, Germany. Electronic mail: leonid.goubergrits@charite.de, goubergrits@dhzb.de

parts of human circulation is able to assess patient-specific physiologic and pathophysiologic flow conditions.^{1,12,19} CFD tools are supposed to support clinicians in making the diagnosis, to help with difficult treatment decisions, and to optimize treatment, especially by predicting the post-treatment changes. Several studies recently showed the applicability of CFD for hemodynamic analysis before the treatment procedure. Wang *et al.* conducted CFD simulations of patient-specific total cavopulmonary connections (TCC) that were used for the surgical repair of single ventricle heart disease.²⁵ They revealed that complex flow structures were related to hemodynamic performance and to the surgical outcome of a TCC. Energy loss in the TCC poses the same problem for the heart as a CoA, both of which are congenital heart diseases. Marsden *et al.* proposed including transient boundary conditions with varying levels of patient exercise in their CFD model. The obtained time-resolved flow field was used to evaluate respiratory and exercise effects on the local hemodynamics within a TCC.¹⁷ Based on these data, they were able to quantify the hemodynamic efficiency of Fontan geometry under different exercise conditions, noting that further development of their technique “[...] could be used in deciding the course of treatment for a particular patient”. Corno *et al.* proved in a combined (CFD, animal and *in vitro* model) study that an assisted Fontan procedure was able to improve hemodynamics (pulmonary flow increase).⁴ Besides evaluating local hemodynamics in vessels and bypasses, CFD calculated flow parameters can also be used in conjunction with specialized optimization algorithms to improve surgery and surgical equipment or to prove a new hypothesis. Marsden published a comprehensive review of the potential and difficulties of CFD-driven optimization programs for medical engineering, citing bypass grafts, stents and Fontan junctions as examples.^{15,16} Their development can significantly benefit from simulation-driven optimization. Some recent studies attracted broad interest, focusing on CFD application in patients with CoA, which is considered a simple disease.¹³ LaDisa *et al.*, for example, performed different CFD simulations comparing the hemodynamics of one normal, two pre- and two postoperative CoA patients.¹³ By comparing the flow fields of the pre- and postoperative and normal aortas, they revealed abnormal wall shear stress (WSS) patterns in both preoperative and postoperative CoA geometries, concluding that “[...] restoring favorable anatomy may not restore normal hemodynamics”. Furthermore, Olivieri *et al.* focused his study on different types of postoperative CoA, and showed that geometric variations result in flow separation variation causing differences in WSS values along the aorta.²¹ WSS is the

major hemodynamic parameter associated with abnormal flow conditions and responsible for the pathological wall remodeling. Midulla *et al.* investigated blood flow within a thoracic stent graft.¹⁸ He found different maps of flow and WSS in different patients, and stated that MRI-based CFD can model aortic hemodynamics for clinical problems. For example, Humphrey noted that the vessel shape is adapted to strive for an optimal WSS.¹⁰ Chiu and Chien showed that low and/or disturbed WSS results in changes in the endothelium that subsequently result in a vulnerable vessel wall that promotes thrombus formation and atherosclerosis development.²

The great interest in CoA is due to the known fact that treatment of the CoA by surgery, endovascular stent placement, or balloon angioplasty cures the blood pressure gradient between the upper and lower extremities, but in the long-term prognosis systemic hypertension frequently persists and is associated with a set of complications (stroke, aneurysm formation and coronary artery disease) known to decrease overall life expectancy.³ The use of CFD in congenital heart disease was recently reviewed by DeCampi *et al.*⁵

The specific aim of this study was to prove the ability of MRI-based CFD tools to improve post-treatment hemodynamics in patients with coarctations of the aorta (CoA) compared with a clinical decision alone.

MATERIALS AND METHODS

Patient Data

The study was performed using data obtained from 13 consecutive patients (6 males, 7 females) with aortic coarctations (three native and the rest re-CoA) treated in the Department of Congenital Heart Disease and Pediatric Cardiology at the German Heart Institute in Berlin, Germany between October 2011 and January 2013. The age range was between 14 and 52 years (mean age of 25 ± 14 years). All patients had clinical indications for catheterization from the preceding Cardiac Magnetic Resonance study. The mean degree of stenosis (DS) was $54.8 \pm 19.21\%$ relating these patients in the mid-sized stenosis group. The mean geometric length of the stenosis was 36.0 ± 8.5 mm. The DS was defined as a ratio of cross-sectional areas:

$$DS = 100\% \times (1 - A_{st}/A_1),$$

where A_{st} is the cross-sectional area at the stenosis and A_1 is the cross-sectional area at the descending aorta measured approximately 150 mm downstream of the aorta inlet. This is a location normally used in clinical practice as a reference value for stenosis enlargement (target post-treatment diameter). All patients were treated with the implantation of a bare CP Stent™

pre-mounted on a BIB[®] (ballon in ballon) Catheter (NuMED Inc., USA), except one patient who was treated with balloon angioplasty and one patient who remained untreated. The treatment is done during catheterization, which includes biplane angiography imaging with a contrast agent and pressure measurements. The x-ray projection images are used to analyze diameters of the aorta and the length of the coarctation. The size (diameter and length) of the selected stent is based on these size evaluations and the site of the CoA. The length of stents used varied between 16 and 45 mm (mean length of 30.69 ± 8.10 mm). Due to treatment, the diameter of the aorta at the stenosis was significantly enlarged from 10.3 ± 2.14 to 16.0 ± 2.55 mm diameter ($p = 0.00$, the paired student's *t*-test according to the Kolmogorov–Smirnov test). We consider the current treatment procedure not optimal, since the stent diameter is selected according to the diameter of the descending aorta. This, however, does not take into account the tapering of the aorta with the significantly different mean diameters of the ascending and descending aortas (26.4 ± 5.18 vs. 16.2 ± 3.15 mm, $p = 0.00$, paired student's *t*-test for normally distributed data) measured in our patients.

The local Institutional Review Board followed the ethical guidelines of the 1975 Declaration of Helsinki. Approval was obtained and informed consent was given by the patients and/or their guardians.

The present study is based on the data of the same cohort of patients used in a recently published study.⁹ This paper describes in detail the imaging data, protocols, device used, segmentation and geometry reconstruction. Briefly, the study is based on 3D whole heart MRI (3DWH) data used for the anatomy assessment and flow-sensitive 4D velocity-encoded magnetic resonance imaging (4D VEC-MRI) data used to set the boundary flow conditions. MRI-measured flow rates in the ascending aorta just above the sinotubular junction and in the descending aorta were used to determine the peak systolic inlet flow rate assuming a plug inlet velocity profile. At the same time, the flow rate in the descending aorta was used to set the outflow boundary conditions. The difference between flow rates in the ascending and descending aortas was distributed between side branches of the aortic arch according to cross-sectional area relationships.¹⁴

The anatomy of the aorta was segmented and reconstructed with the software ZIBAmira (Zuse Institute Berlin, Germany) as described previously.⁸ MRI-based flow data (flow rates in the ascending and descending aortas) were analyzed using GTFlow 1.6.8 software (Gyrotools, Zurich, Switzerland).

The present CFD study used the same working pipeline as the previous study.⁹ In this clinical validation study, CFD-predicted pre- and post-treatment

peak systole pressure drops through aortic coarctation were successfully validated against catheterization-based pressure measurements. In our earlier study, we showed a good correlation between MRI-measured and CFD-calculated flow fields, as visualized by path lines.⁸ Briefly, patient-specific steady peak systole flow conditions were analyzed with the software ANSYS[®] Fluent[®] 14.5 (ANSYS Inc., USA). A non-Newtonian blood model was applied using an adapted power law model as described earlier,²⁶ assuming a blood density of 1050 kg/m^3 , hematocrit value of 40%, blood temperature of $37 \text{ }^\circ\text{C}$ and total protein albumin difference value of 27 g/L . A $k-\omega$ SST transition turbulence model assuming low aorta inlet turbulence intensity of 5% was used. This turbulence model has some limitations for the assessment of turbulence parameters. The major hemodynamic parameters evaluating CoA in clinical practice (the pressure drop) is, however, independent of turbulence parameters.¹¹ The used turbulence model is also correctly assesses mean velocity field and thus WSS.²⁴ At all outlets far from the coarctation, the Fluent-implemented outlet boundary condition “outflow” applying a zero diffusion flux for all flow variables and an overall mass balance correction was used. This means that the conditions of the outflow plane are extrapolated from within the domain and have no impact on the upstream flow. We checked also the absence of recirculations at all outlets. Pre-, post- and virtual treatment simulations were performed with the same flow conditions measured pre-treatment by MRI. High quality unstructured volume meshes accounting for ≈ 2 Million cells varying with the volume of the aorta were fabricated with the Gambit software (ANSYS Inc., USA) following requirements of the simulated flow regime (turbulence) and a previous mesh independence study. A double-precision solver with the second-order discretization scheme and SIMPLEC for the pressure–velocity coupling was used. Convergence criteria were set to residual errors $< 10^{-5}$.

The statistical analysis of morphometric and hemodynamic parameters was conducted with SPSS[®] software (version 21, IBM Inc., USA). Data are expressed as the mean \pm the standard deviation (SD). Significance was assumed to be $p \leq 0.05$ for all tests.

Virtual Treatment

The fabrication of the virtual treatment geometry was aligned with the segmented label field of MRI-based (Fig. 1a) pre-treatment aorta anatomy. The working pipeline was developed with the software ZIBAmira and visualized in Fig. 1. The label field of the pre-treatment anatomy (Fig. 1b) was first used to generate the smoothed triangulated surface of the

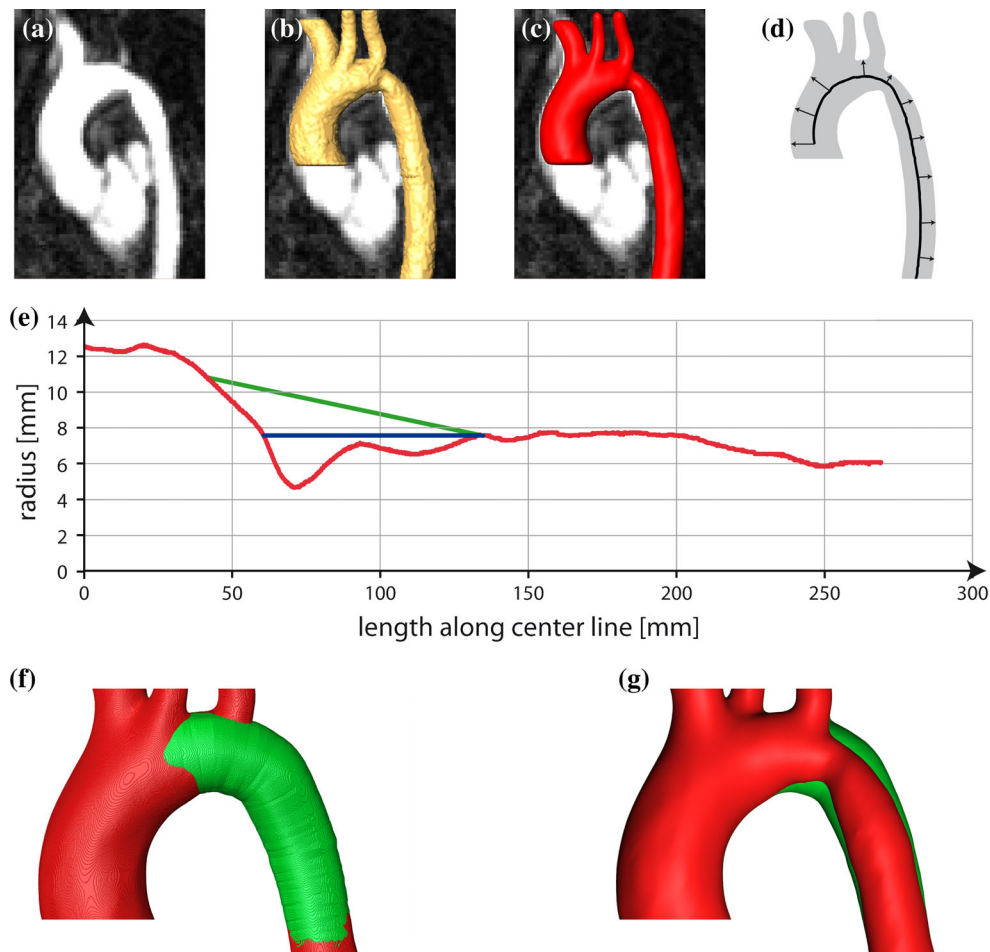


FIGURE 1. Workflow of the virtual treatment procedure using MRI data (a), the segmentation procedure (b), geometry surface generation (c), center line analysis including surface distance (diameter) calculation (d), virtual treatment (new course and diameter enlargement of the aorta) (e), label field of the treatment generation and the merging of the pre-treatment label field (f) with the final geometry generation, including the smoothing procedure (g). The diameter course (e) includes pre-treatment (red line), post-treatment (blue line) and virtual treatment (green line) data.

aorta (Fig. 1c). This same label field was also used to automatically generate the aorta's center line. The surface distance tool automatically calculated the averaged cross-section radii of the aorta along the center line (Fig. 1d). The resulting radius curve is used to propose a virtual treatment aiming to reconstruct the smooth tapering course of the radius curve as shown in Fig. 1e (green line), while at the same time keeping the length of the treated segment as short as possible. In contrast, the clinical treatment procedure tried to enlarge the stent to the constant diameter of the descending aorta, as shown in Fig. 1e (blue line). The label field of the virtual treatment segment with a resolution of $0.7 \times 0.7 \times 0.7 \text{ mm}^3$ was then generated using the 3D center line course of the pre-treatment label field and the diameters of the corresponding green line. Afterwards, both label fields were merged (Fig. 1f) and a smooth surface of the virtual treatment geometry was generated as a result. Figure 1g shows

both reconstructed surfaces of the pre- and virtual treatment (partially transparent surface visualization) geometry.

RESULTS

Virtual treatments of aortic coarctations caused significant dilatation of the stenosis diameter from 10.3 ± 2.14 to 18.7 ± 3.24 mm. The virtual stenosis enlargement was approximately 1.5 times higher than was achieved by a patient treatment with an average target diameter for the stenosis of 16.0 ± 2.55 mm. The average length of the treated aorta segment was 92.7 ± 30.99 mm or three times the average stent length (30.69 ± 8.10 mm).

On average, virtual treatment allowed an improvement (reduction) in the pressure drop through aortic coarctation by an additional 2.8 ± 3.15 mmHg com-

pared with the pressure drop reduction achieved through clinical treatment (6.7 ± 5.58 mmHg post-treatment pressure drop as calculated by CFD). The improved pressure drop was achieved in a majority (10/13) of cases. Figure 2 represents pre-, post- and virtual treatment courses along the aorta's length of relative static pressures and aortic diameters.

Furthermore, we analyzed the average cross-sectional WSS values at the stenosis segment. The stenosis segment was defined at 20 mm aortic length upstream and 40 mm aortic length downstream of the stenosis site. Figure 3 shows cross-sectional WSS curves averaged (mean and median curves) over all 13 cases of aortic coarctation investigated. Virtual treatment significantly reduced cross-sectional peak WSS at the stenosis site relative to both pre- and post-treatment situations: virtual treatment $34.9/35.0 \pm 15.15$ Pa (mean/median \pm SD) vs. pre-treatment $17.5/12.6 \pm 13.51$ Pa ($p = 0.00$) and post-treatment $11.8/7.5 \pm 9.99$ Pa ($p = 0.00$) by the paired Wilcoxon test and/or Kolmogorov–Smirnov test. Analysis of the WSS values for the segments was carried out by averaging the mean and median curves shown in Fig. 3. This analysis also found a significant reduction

in WSS ($p < 0.05$, paired student's *t*-test and/or Kolmogorov–Smirnov test) suggested by virtual treatment for both pre- and post-treatment situations (Table 1).

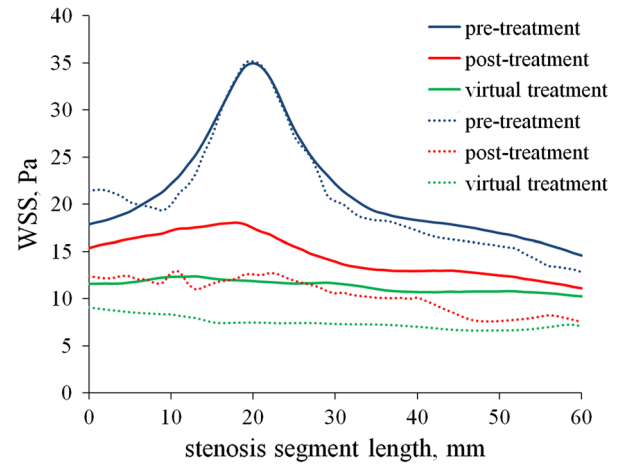


FIGURE 3. Cross-sectional WSS courses (pre-, post- and virtual treatment) averaged (mean—solid line and median—dotted line) over 13 cases. The averaging included an alignment of all patient-specific WSS courses: all stenosis sites were aligned with the 20 mm location.

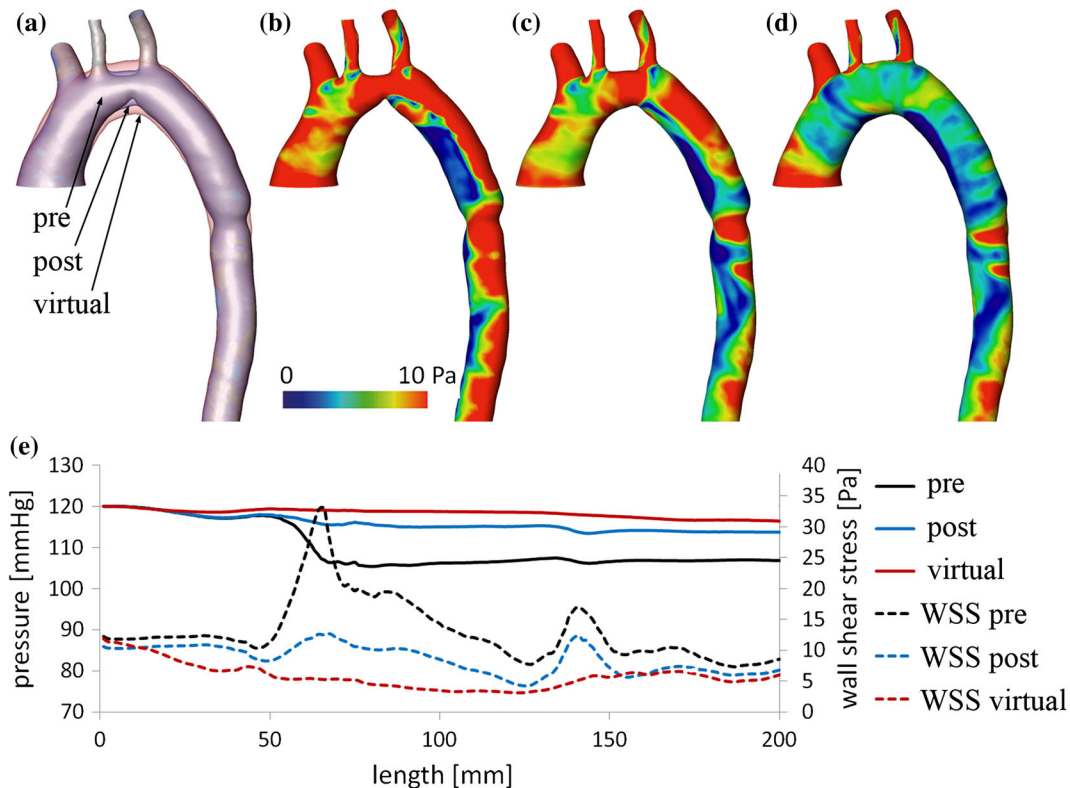


FIGURE 2. Representation of pre-, post- and virtual treatment geometries (pre—grey color; post—transparent blue color; virtual—transparent red color) as 3D overlapped surfaces (a), WSS distributions of pre- (b), post- (c) and virtual treatment (d) geometries. Curves show averaged cross-sectional courses of static pressures (solid lines) and WSS values (dotted lines) along the aorta center line (e). Black lines represent pre-treatment hemodynamics, whereas blue and red lines represent post- and virtual treatment situations, respectively. An improvement of hemodynamics from pre- to post- and virtual treatment is seen.

The improvement (reduction) in WSS in the stenosis segment 60 mm in length as proposed by virtual treatment instead of the post-treatment option correlates significantly ($p = 0.00$) with the reduction in pressure drop. The linear regression analysis found a Pearson r -square coefficient of $r^2 = 0.83$.

DISCUSSION

The study compares peak systole hemodynamics (pressure drops and WSS) calculated by CFD in pre-treatment, post-treatment and virtual treatment geometries in 13 patients with coarctations of the aorta. We found that virtual treatment as proposed by engineers could significantly improve the pressure drop and aortic WSS if compared to both pre- and post-treatment situations. The improvement of the pressure drop relative to the post-treatment geometry, however, is relatively small considering the accuracy of catheterization. This is also because the post-treatment geometry usually exhibits a very small rest-stenosis along with a low pressure drop.¹¹ The accuracy of catheterization pressure measurement should be below 3% as per the ISO norm (IEC 60601-2-34:2000). This would mean an accuracy of 3.6 mmHg for each 120 mmHg of pressure measured. Consequently, the improvement in the pressure drop proposed by virtual treatment cannot be validated as opposed to clinical

practice (post-treatment) using the catheterization technique. Current clinical threshold levels for re-intervention are also usually higher. However, it remains unclear how an additional reduction in the pressure gradient would contribute to a longer period between interventions, as this would also decrease hospitalization and interventional risks for the individual patient. Also, catheterization is currently the clinical reference standard for treatment decisions and evaluation.

In contrast, the impact of virtual treatment on WSS improvement was much higher. This is not surprising, since WSS is known to be the most sensitive parameter compared to pressure or velocity fields.²² The WSS could be accurately assessed only by CFD, thus challenging the validation of our findings in clinical settings.

The improved hemodynamics due to virtual treatment has a price: the target diameter of the stenosis enlargement in virtual treatment was on average 2.7 mm larger than that of post-treatment. Furthermore, the length of the segment treated virtually was much higher (three times) than the stent length used. This kind of a treatment procedure also means a higher treatment risk. The average stent length correlates very well with the geometric length of the stenosis (30.7 vs. 36 mm). The analysis of average cross-sectional WSS curves (Fig. 3) shows that the impact of the stenosis on WSS (WSS increase) is

TABLE 1. WSS values averaged over all investigated cases and stenosis segments.

	Pre-treatment (Pa)	Post-treatment (Pa)	Virtual treatment (Pa)
Mean curves	21.5 ± 5.68	14.5 ± 2.19	11.4 ± 0.62
Median curves	24.5 ± 6.11	11.3 ± 1.82	7.5 ± 0.67

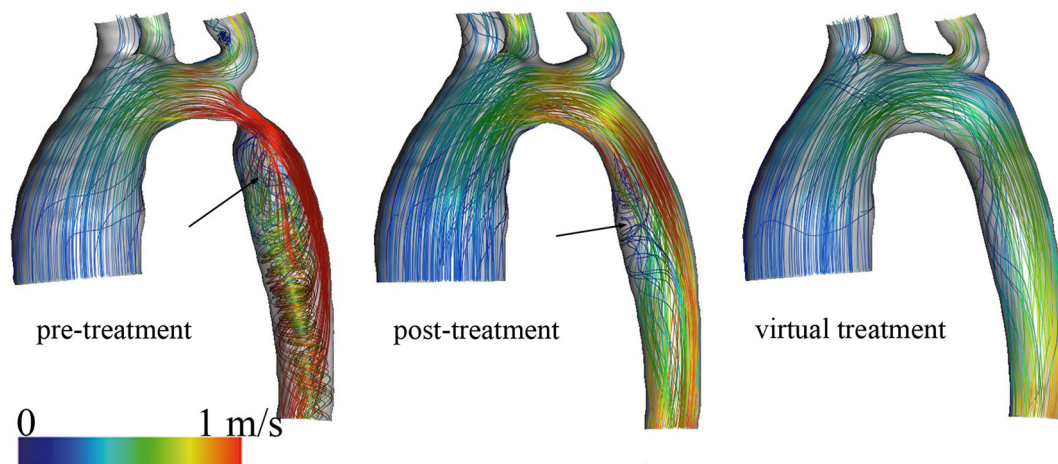


FIGURE 4. Representation of path lines color-coded by velocity magnitude for pre-, post- and virtual treatment simulations of one patient. The path lines show that a treatment procedure (clinical decision) does not completely eliminate the post-stenosis recirculation region. This was, however, achieved following the virtual treatment. Black arrows mark recirculation regions.

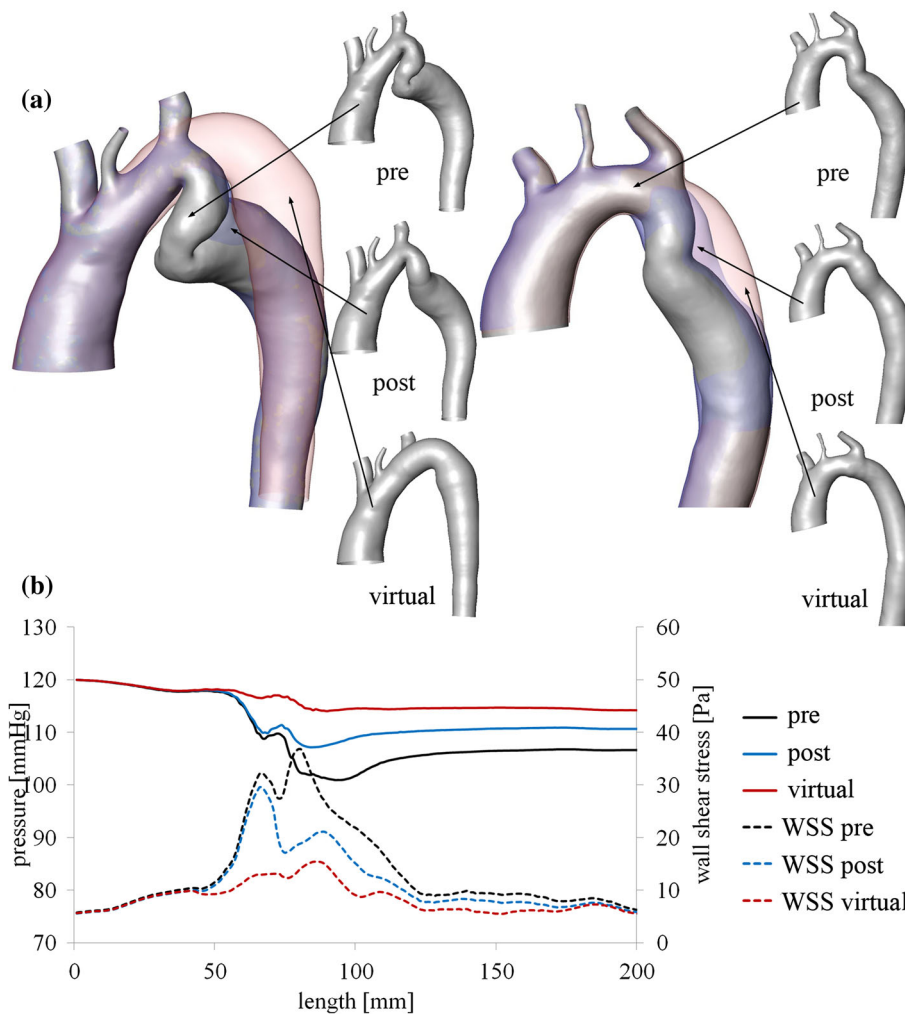


FIGURE 5. (a) Two cases of the pre- (grey color), post- (transparent blue color), and virtual treatment (transparent red color) geometries with very complex courses of the aorta corrected by virtual treatment. (b) Average cross-sectional courses of static pressures (solid lines) and WSS values (dotted lines) along the center line for the first case shown above. Black lines represent pre-treatment hemodynamics, whereas blue and red lines represent post- and virtual treatment situations, respectively.

much higher. The WSS increase was observed averaged along a segment at least 60 mm in length. Hence, if the treatment procedure aims to improve WSS and restore physiological WSS, a much longer segment of the aorta should be treated. The significantly larger aortic segment proposed for treatment by engineers is associated with another open question in this study—the treatment option. In some cases, virtual treatment could not be realized by intravascular treatment (stent placement and/or balloon angioplasty): a longer stent could in some cases cover an ostium of an aortic arch side branch that is deemed dangerous for a patient. In these cases, surgical treatment (e.g., resection, end-to-end anastomosis, or patch aortoplasty) associated with longer hospitalization and more complications⁶ would have to be considered. A use of the aorta prosthesis (e.g., Vascutek® Gelweave™ Plexus Grafts, Vascutek

Ltd., UK) allows replacing surgically the whole deceased aorta including also the aortic arch.

In this study, the primary WSS analysis was focused on the average cross-sectional WSS values, which were pathologically increased due to stenosis. There is also another aspect, a development of the post-stenosis recirculation regions associated with very low WSS values. Recirculation regions are well known to be associated with abnormal hemodynamics. We stated that treatment procedures eliminated the post-stenosis recirculation only in few cases. In contrast, the virtual treatment procedure was able to eliminate or significantly reduce this flow feature in all 10 cases where virtual treatment improved hemodynamics compared to a post-treatment situation. Figure 4 exemplifies such an improvement. In some cases, the significant improvement in the aortic hemodynamics was achieved due to a correction of the aortic course (Fig. 5a). Figure 5b

shows the significantly improved hemodynamics due to a virtual treatment proposed by an engineer. This is because flow recirculation develops not only behind a stenosis. Curved or kinked vessel segments could also promote this abnormal hemodynamics. This also explains why, in two cases, virtual treatment did not improve hemodynamics compared to a clinical post-treatment situation. Virtual treatment improved hemodynamics only in 10 out of 13 of the cases. In a third case, the clinical decision was simply ideal. The elimination of the recirculation region at the stenosis segment could be a good treatment target and thus validation parameter for treatment success. This can be assessed non-invasively by a 4D VEC-MRI and thus used to prove the advantage of CFD-based virtual treatment.

The CFD study is associated with some limitations due to technical (clinically measured patient-specific flow parameters), physiologic or software-related errors. These limitations possibly affecting the CFD results were discussed extensively in earlier studies.^{1,7,8,20} Finally, the findings presented here only represent a change in aortic hemodynamics due to a change in the aorta geometry (treatment of the coarctation). All other effects of treatment (possible change in cardiac output, flow rate ratio between the descending aorta and side branches or aortic compliance, which also affects flow rates) were not considered in this study. The focus of this study was a peak systole hemodynamics. The differences in hemodynamics found between pre-, post- and virtual treatment geometries could differ during other phases of the cardiac cycle. In future studies the analysis of the cardiac cycle assessing time-dependent flow characteristic is planned.

CONCLUSION

CFD-based analysis based on non-invasive patient-specific imaging data, for example MRI, has a huge potential to improve post-treatment hemodynamics associated with poor long-term prognosis of patients with CoA. The target parameter to be improved by CFD is WSS, whereas the target diagnosis parameter, the pressure drop, is less sensitive at very low degrees of stenosis. The impact of the WSS improvement for patient outcome should be proven in a long-term clinical study.

ACKNOWLEDGMENTS

This study was supported by the German Research Foundation (DFG).

REFERENCES

- ¹Arbia, G., C. Corsini, M. Esmaily Moghadam, A. L. Marsden, G. Migliavacca, T. Y. Pennati, I. E. Hsia, and Modeling of Congenital Hearts Alliance (MOCHA) Investigators. Numerical blood flow simulation in surgical corrections: what we need for an accurate analysis? *J. Surg. Res.* 186(1):44–55, 2014.
- ²Chiu, J. J., and S. Chien. Effects of disturbed flow on vascular endothelium: pathophysiological basis and clinical perspectives. *Physiol. Rev.* 91(1):327–387, 2011.
- ³Cohen, M., V. Fuster, P. M. Steele, D. Driscoll, and D. C. McGoon. Coarctation of the aorta. Long-term follow-up and prediction of outcome after surgical correction. *Circulation* 80:840–845, 1989.
- ⁴Corno, A. F., C. Vergara, C. Subramanian, R. A. Johnson, T. Passerini, A. Veneziani, L. Formaggia, N. Alphonso, A. Quarteroni, and J. C. Jarvis. Assisted Fontan procedure: animal and *in vitro* models and computational fluid dynamics study. *Interact. Cardiovasc. Thoracic Surg.* 10:679–684, 2010.
- ⁵DeCampli, W. M., I. R. Arqueta-Morales, E. Divo, and A. J. Kassab. Computational fluid dynamics in congenital heart disease. *Cardiol. Young* 22(6):800–808, 2012.
- ⁶Forbes, T. J., D. W. Kim, W. Du, D. R. Turner, R. Holzer, Z. Amin, Z. Hijazi, A. Ghasemi, J. J. Rome, D. Nykanen, E. Zahn, C. Cowley, M. Hoyer, D. Waight, D. Gruenstein, A. Javois, S. Foerster, J. Kreutzer, N. Sullivan, A. Khan, C. Owada, D. Hagler, S. Lim, J. Canter, and T. Zellers. Comparison of surgical, stent, and balloon angioplasty treatment of native coarctation of the aorta: an observational study by the CCISC (Congenital Cardiovascular Interventional Study Consortium). *J. Am. Coll. Cardiol.* 58:2664–2674, 2011.
- ⁷Goubergrits, L., U. Kertzscher, B. Schöneberg, E. Wellenhofer, Ch. Petz, and H.-Ch. Hege. CFD analysis in an anatomically realistic coronary artery model based on non-invasive 3D imaging: comparison of magnetic resonance imaging with computed tomography. *Int. J. Cardiovasc. Imaging* 24:411–421, 2008.
- ⁸Goubergrits, L., R. Mevert, P. Yevtushenko, J. Schaller, U. Kertzscher, S. Meier, S. Schubert, E. Riesenkampff, and T. Kuehne. The impact of MRI-based inflow for the hemodynamic evaluation of aortic coarctation. *Ann. Biomed. Eng.* 41:2575–2587, 2013.
- ⁹Goubergrits, L., E. Riesenkampff, P. Yevtushenko, J. Schaller, U. Kertzscher, A. Hennemuth, F. Berger, S. Schubert, and T. Kuehne. MRI-based computational fluid dynamics for diagnosis and treatment prediction: clinical validation study in patients with coarctation of aorta. In press, doi: [10.1002/jmri.24639](https://doi.org/10.1002/jmri.24639), 2014.
- ¹⁰Humphrey, J. D. Vascular adaptation and mechanical homeostasis at tissue, cellular, and sub-cellular levels. *Cell Biochem. Biophys.* 50(2):53–78, 2008.
- ¹¹Itu, L., P. Sharma, and K. Ralovich. Non-invasive hemodynamic assessment of aortic coarctation: validation with *in vivo* measurements. *Ann. Biomed. Eng.* 41:669–681, 2013.
- ¹²LaDisa, J. F., C. A. Taylor, and J. A. Feinstein. Aortic coarctation: recent developments in experimental and computational methods to assess treatments for this simple condition. *Prog. Pediatr. Cardiol.* 30(1):45–49, 2010.
- ¹³LaDisa, Jr., J. F., C. Alberto Figueroa, I. E. Vignon-Clementel, H. J. Kim, N. Xiao, L. M. Ellwein, F. P. Chan, J. A. Feinstein, and C. A. Taylor. Computational simula-

- tions for aortic coarctation: representative results from a sampling of patients. *J. Biomech. Eng.* 133(9):091008, 2011.
- ¹⁴Lantz, J., and M. Karlsson. Large eddy simulation of LDL surface concentration in a subject specific human aorta. *J. Biomech.* 45:537–542, 2012.
- ¹⁵Marsden, A. L. Simulation based planning of surgical interventions in pediatric cardiology. *Phys. Fluids.* 25(10):101303, 2013.
- ¹⁶Marsden, A. L. Optimization in cardiovascular modeling. *Ann. Rev. Fluid Mech.* 46:519–546, 2014.
- ¹⁷Marsden, A. L., I. E. Vignon-Clementel, F. P. Chan, J. A. Feinstein, and C. A. Taylor. Effects of exercise and respiration on hemodynamic efficiency in CFD simulations of the total cavopulmonary connection. *Ann. Biomed. Eng.* 35(2):250–263, 2007.
- ¹⁸Midulla, M., R. Moreno, A. Baali, M. Chau, A. Negre-Salvayre, F. Nicoud, J. P. Pruvo, S. Haulon, and H. Rousseau. Haemodynamic imaging of thoracic stent-grafts by computational fluid dynamics (CFD): presentation of a patient-specific method combining magnetic resonance imaging and numerical simulations. *Eur. Radiol.* 22(10):2094–2102, 2012.
- ¹⁹Morbiducci, U., R. Ponzini, D. Gallo, C. Bignardi, and G. Rizzo. Inflow boundary conditions for image-based computational hemodynamics: impact of idealized versus measured velocity profiles in the human aorta. *J. Biomech.* 46(1):102–109, 2013.
- ²⁰Nordmeyer, S., E. Riesenkampff, G. Crelier, A. Khasheei, B. Schnackenburg, F. Berger, and T. Kuehne. Flow-sensitive four-dimensional cine magnetic resonance imaging for offline blood flow quantification in multiple vessels: a validation study. *J. Magn. Reson. Imaging* 32:677–683, 2010.
- ²¹Olivieri, L. J., D. A. de Zélicourt, C. M. Haggerty, K. Ratnayaka, R. R. Cross, and A. P. Yoganathan. Hemodynamic modeling of surgically repaired coarctation of the aorta. *Cardiovasc. Eng. Technol.* 2(1):288–295, 2011.
- ²²Prakash, S., and C. R. Ethier. Requirements for mesh resolution in 3-D computational hemodynamics. *J. Biomech. Eng.* 123(2):134–144, 2001.
- ²³Rourke, M. F., and T. B. Cartmill. Influence of aortic coarctation on pulsatile hemodynamics in the proximal aorta. *Circulation* 44(2):281–292, 1971.
- ²⁴Ryval, J., A. G. Straatman, and D. A. Steinamn. Two-equation turbulence modeling of pulsatile flow in a stenosed tube. *J. Biomech. Eng.* 126(5):625, 2004.
- ²⁵Wang, C., K. Pekkan, D. De Zélicourt, M. Horner, A. Parihar, A. Kulkarni, and A. P. Yoganathan. Progress in the CFD modeling of flow instabilities in anatomical total cavopulmonary connections. *Ann. Biomed. Eng.* 11:1840–1856, 2007.
- ²⁶Wellnhofer, E., J. Osman, U. Kertzsch, K. Affeld, E. Fleck, and L. Goubergrits. Flow simulation studies in coronary arteries—Impact of side-branches. *Atherosclerosis* 213:475–481, 2010.